C. R. Chimie 21 (2018) 862–871

Contents lists available at ScienceDirect

Comptes Rendus Chimie

www.sciencedirect.com

Full paper/Mémoire

Nanostructured ternary composites of PPy/CNT/$NiFe_2O_4$ and PPy/CNT/$CoFe_2O_4$: Delineating and improving microwave absorption

Erfan Ghashghaei [a], Somayyeh Kheirjou [b, *], Sara Asgari [c], Hanif Kazerooni [a]

[a] Department of Chemistry, Amirkabir University of Technology, Tehran, Iran
[b] Department of Chemistry, Sharif University of Technology, Tehran, Iran
[c] Department of Chemistry, Karaj Branch, Islamic Azad University, Karaj, Iran

ARTICLE INFO

Article history:
Received 22 July 2017
Accepted 15 May 2018
Available online 19 June 2018

Keywords:
Microwave reflection loses
Polypyrrole
Nanocomposite
Carbon nanotube
CNT

ABSTRACT

Two different ternary nanocomposites, PPy/CNT/$CoFe_2O_4$ and PPy/CNT/$NiFe_2O_4$, were synthesized by in situ polymerization method. The resulting composites were characterized using Fourier transform infrared spectroscopy, transmission electron microscopy, scanning electron microscopy, energy-dispersive spectroscopy, and X-ray diffraction. They were evaluated with the aim of investigating microwave absorption properties. The results showed that the value of microwave reflection decreases as that of prepared nanocomposites increases. This happens with increase in the PPy content and polymerization on the surface.

1. Introduction

Whether intrinsically conducting or in the composite form, conducting polymers have always been and probably will always be viewed as a highly relevant field of research. Innumerable articles have been published on their chemical, electrical, and mechanical properties. Microwave properties, however, are receiving considerable attention [1,2]. In recent years, microwave absorption technology as electromagnetic (EM) interference has sparked interest from a new point of view, and EM pollution has become a vital concern [3,4]. Besides adversely effecting industrial equipment, EM pollution also damages the health of living beings by breaking down DNA strands, accelerating heart rates, causing cancer, and so forth [5–7]. Thus, finding more effective materials that can absorb these EM or microwave radiations is indispensable [8].

Considerable interest has been directed onto composite materials with conducting and magnetic properties. These materials have potential applications in numerous fields. They have superior properties with synergistic or complementary behaviors between conducting polymers and inorganic magnetic nanoparticles [1]. There are many types of such materials, such as Ni [9,10], Co [10], Fe_2O_3 [11,12], Fe_3O_4 [13–15], $CoFe_2O_4$ [16], $NiFe_2O_4$, Co_3O_4, and $BaFe_{12}O_{19}$. These materials can all be operated as magnetic portions of the composite materials [17]. Ferrite (MFe_2O_4, M = Co^{2+}, Ni^{2+}, Fe^{2+}, Zn^{2+}, Cu^{2+}, etc.) nanocrystals have received considerable interest because of their potential application in diverse parts of chemistry, such as ferrofluids [18–20], magnetic fluids [21], magnetic recording media [22], and magnetic resonance imaging [23,24]. Among magnetic materials, the spinel ferrites show significant magnetic properties and can be used widely, examples

* Corresponding author.
E-mail address: Somayyehkheirjou@gmail.com (S. Kheirjou).

https://doi.org/10.1016/j.crci.2018.05.003
1631-0748/

include radio-frequency regions, and in achieving physical flexibility, high electrical resistivity, mechanical hardness, and chemical stability [25]. Their properties get enhanced only when the particle size reaches the nanometer range [26]. $NiFe_2O_4$ is one of the most important magnetic ferrites, which has a range of applications in diverse areas, such as permanent magnets, ferrofluids, and gas sensors. Among ferrites, cobalt ferrite ($CoFe_2O_4$) is especially interesting because of its special magnetic properties such as strong anisotropy, high coercivity at room temperature, and moderate saturation magnetization, and its nanoparticles have known to be a photomagnetic material [27,28]. Its properties are over-reliant on the methods used for the synthesis [29].

On the other hand, many conducting polymers such as polyaniline (PANI) [30–32], polypyrrole (PPy) [12,13,33,34], polythiophene [35], polyacetylene, and their derivatives can be used as the conducting part of composite materials. Brezoi and Ion [36] had reported the preparation of nanocomposites of PPy and iron oxide by a simultaneous gelation and polymerization method. Bao and Jiang [37] had prepared the nanocomposites of PANI and iron oxide by high-energy ball milling [17].

In addition to these two-component composites, many different experimental methods for the synthesis of three-component composites relying on the carbon material have been developed and practiced, these aim to obtain a definite objective in EM shielding and attenuation [38,39]. For instance, Cao et al. [38] had reported preparation of three-component PANI/Fe_3O_4/carbon nanotube (CNT) composites with remarkable microwave absorption properties. Liu et al. [39] found that PPy-reduced graphene oxide–Co_3O_4 developed with strong microwave absorption properties [8]. Luo and co-workers have investigated the synthesis, characterization, and microwave absorption properties of ternary composites of reduced graphene oxide, different magnetic particles (such as Fe_3O_4 porous nanospheres, carbonyl iron powders, and strontium ferrite), and PANI. They have used the reduced graphene oxide because of its high specific surface area and excellent electronic conductivity. They have shown that the aforementioned synthesized ternary composites have excellent microwave absorption properties [40–43].

It is clear and could be deduced from the literature, the complex permittivity affected by the presence of a conductive polymer layer on the surface of nanoparticles and characteristic impedance associated relaxation process modulates by it. Then efficiency of microwave absorption of the material may be controlled by such changes in the complex permittivity and the relaxation process [44]. Therefore, to develop the potential microwave absorbers, which can work in the given frequency range, it is mandatory to get systematic knowledge about the role of conductive polymers on the surface of nanoparticles.

Because of the above-mentioned reasons and as a part of our ongoing research program, we conducted a research on the design and synthesis of three-component composites and investigation of their microwave properties. Here, we report the synthesis of PPy/CNT/$NiFe_2O_4$ and PPy/CNT/$CoFe_2O_4$ nanocomposites.

2. Experimental section

2.1. Solvents and reagents

All reagents were used as received without further purification, unless otherwise mentioned. All reagents and solvents were purchased from Merck (Germany) and Sigma–Aldrich Company, unless otherwise noted.

2.2. Equipment for characterization

Fourier transform infrared (FT-IR) spectra were recorded using a Shimadzu Varian 4300 spectrophotometer in KBr pellets. The crystalline structures of a sample were characterized by an X-ray diffraction (XRD) pattern using a X-ray diffractometer with Ni-filtered Cu Kα radiation (RIGAKU, model D-max C III). The weight percent of magnetic nanoparticles in the synthesized nanocomposites and concentrations were quantified using inductively coupled plasma–optical emission spectroscopy (ICP-OES; Spectro, Arcos). The emergent morphology was observed by scanning electron microscopy (SEM; Philips XL-30 ESEM) and transmission electron microscopy (TEM; Philips EM208, 200 kV). Room temperature magnetic properties were investigated using an alternating gradient force magnetometer device (Meghnatis Daghigh Kavir Company) in an applied magnetic field sweeping between ±10,000 Oe. Reflection loss data were obtained with HP 8510B Network Analyzer (Hewlett–Packard). Thermogravimetric analysis (TGA) was carried out by using a TGA-50H (Shimadzu Corporation, Kyoto, Japan). Metal concentrations were quantified using ICP-OES (Spectro).

2.3. Synthesis of PPy

Pyrrole used as a monomer was distilled three times before use. All reactions were conducted at a temperature of 5 °C. The solution of the oxidizing agent, anhydrous ferric chloride ($FeCl_3$), was used in the ratio of 1:1 (monomer/oxidant). Methanol as a solvent was purified by distillation before use. Pyrrole was added at once to a mixture of $FeCl_3$ and methanol and kept for 4 h at a temperature of 5 °C with constant stirring. PPy obtained as a black powder was filtered by centrifuge and washed with methanol several times to remove any impurities present. The obtained PPy was dried under vacuum at 40 °C for 12 h [45].

2.4. Synthesis of PPy/CNT nanocomposites

To prepare PPy/CNT nanocomposite, 30 wt % CNT was added to the prepared $FeCl_3$ solution. After constantly stirring for 30 min, pyrrole was added at once to the reaction mixture. Then, obtained black precipitate was filtered and washed as per aforementioned procedure.

The same synthesis route was used in the preparation of PPy/$CoFe_2O_4$, PPy/$NiFe_2O_4$, PPy/CNT/$CoFe_2O_4$, and PPy/CNT/$NiFe_2O_4$: 30 wt % of each magnetic material and each carbon structure were added to the prepared $FeCl_3$ solution, and the other steps were completed based on the PPy/CNT nanocomposite synthesis method.

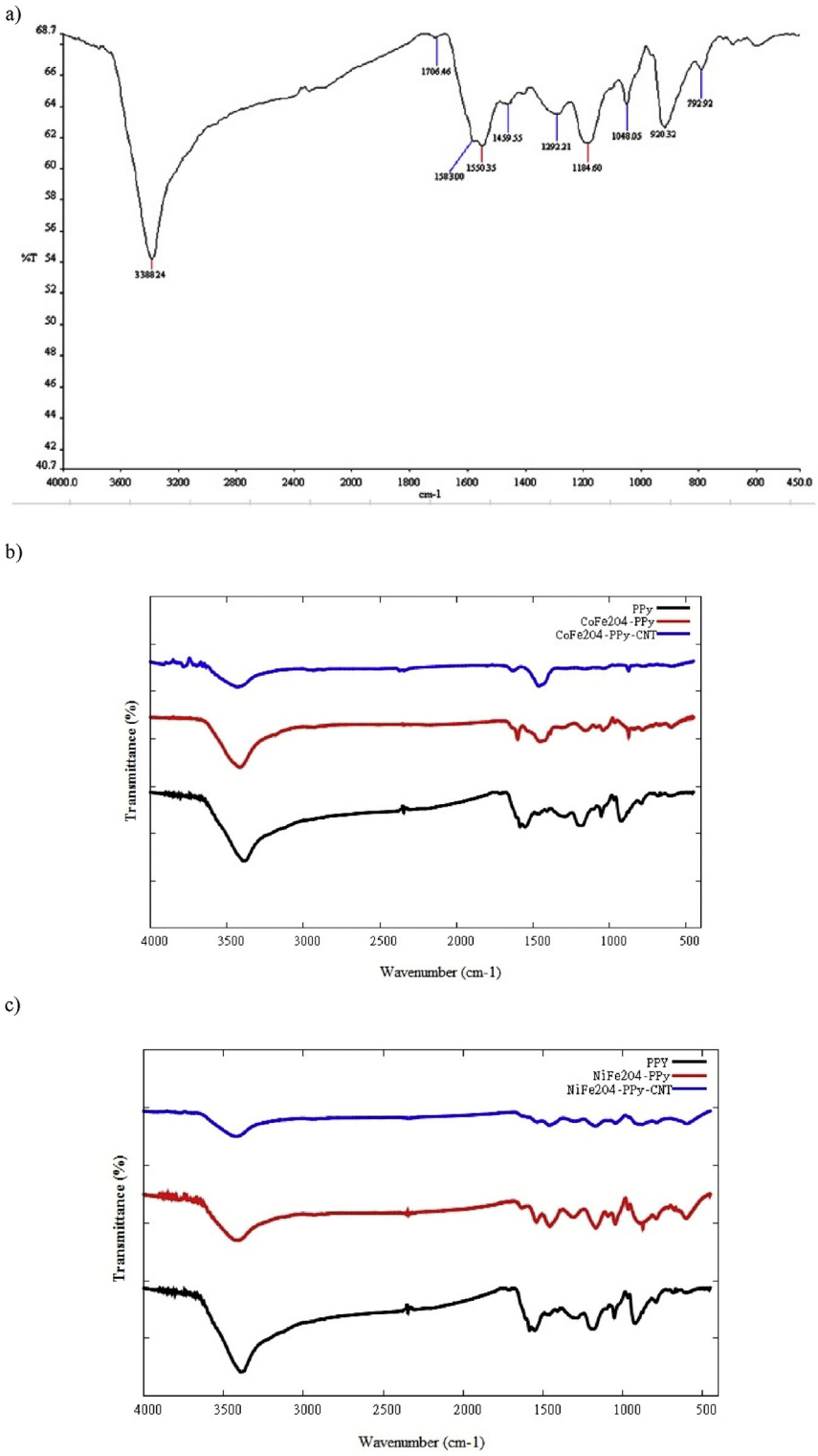

Fig. 1. FT-IR spectra of (a) PPy, (b) PPy/$CoFe_2O_4$ and PPy/CNT/$CoFe_2O_4$, and (c) PPy/$NiFe_2O_4$ and PPy/CNT/$NiFe_2O_4$.

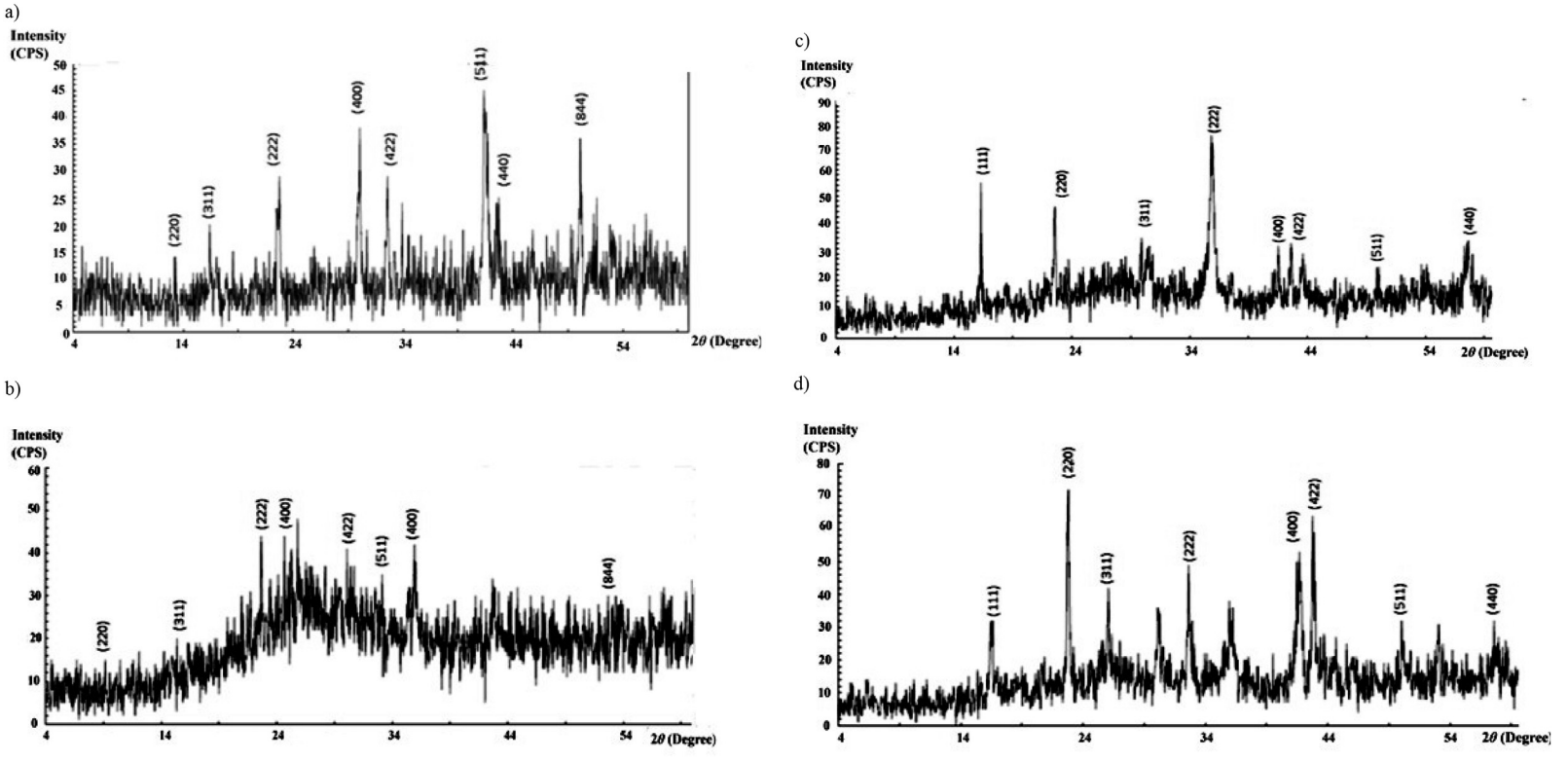

Fig. 2. XRD curves of (a) PPy/$CoFe_2O_4$, (b) PPy/CNT/$CoFe_2O_4$, (c) PPy/$NiFe_2O_4$, and (d) PPy/CNT $NiFe_2O_4$.

3. Results and discussion

3.1. Characterization

3.1.1. FT-IR spectroscopy

The chemical compositions of prepared PPy, PPy/CNT/$CoFe_2O_4$, and PPy/CNT/$NiFe_2O_4$ were evaluated by FT-IR spectroscopy. According to Fig. 1, the characteristic peaks at ~1550, 1459, 1292, 1048, and 920 cm^{-1} are considered to confirm the chemical composition of PPy [46]. The peaks at ~1550 and 1459 cm^{-1} represent pyrrole ring and conjugated CeN stretching, respectively, whereas the peaks at ~1048 and 920 cm^{-1} represent the out-of-plane vibrations of CeH and ring deformation. Fig. 1 quite clearly discloses that PPy/CNT/$CoFe_2O_4$ and PPy/CNT/$NiFe_2O_4$ composites have the characteristic peaks of PPy entities. These results confirm the presence of PPy polymeric moieties in the composite materials. However, a small shift by 5–30 cm^{-1} at the character peak of PPy/CNT/$CoFe_2O_4$ and PPy/CNT/$NiFe_2O_4$ composites can be observed when compared with the curve of PPy, which indicates the interaction between reaction mixture and PPy [47].

3.1.2. X-ray diffraction analysis

The crystalline structures of the samples were determined by the XRD pattern. XRD has a good potential in the analysis of nanostructures because the diffraction patterns yield information about the building materials (sizes of crystallites, microstrain of a lattice, dislocation structures, etc.). There are numerous methods to analyze the XRD line profiles. The most widely applied methods are the Scherrer, Williamson–Hall, and Warren–Averbach methods [48].

Fig. 2 presents the XRD patterns of the prepared PPy/$CoFe_2O_4$, PPy/CNT/$CoFe_2O_4$, PPy/$NiFe_2O_4$, and PPy/CNT/$NiFe_2O_4$ composites. As shown in Fig. 2a, the main characteristic peaks of the X-ray patterns of PPy/$CoFe_2O_4$ are located at $2\theta = 13.56$ (220), 17.21(311), 22.80 (222), 30.05 (400), 33.39 (422), 41.38 (511), 43.51 (440), and 52.46 (844). All these diffraction peaks are related to the $CoFe_2O_4$ structure and can be indexed to the inverse spinel with face-centered cubic pattern [17]. There are two other peaks at 20.8 and 29.5° related to the PPy compound. Diffraction peaks assigned to CNT at $2\theta = 26.58$ can be clearly seen in the XRD curves of PPy/CNT/$CoFe_2O_4$. The XRD pattern of PPy/$NiFe_2O_4$ shown in Fig. 2c refers to a product that has a spinel structure. It is also observed that the crystalline structure of $NiFe_2O_4$ does not change with the addition of PPy. Two broadband diffraction patterns, which are observed at $2\theta = 20.8$ and 25.5, are related to the PPy chains, which are arranged alternately in a vertical and parallel manner.

In this work, the Scherrer equation was used to obtain the crystalline size of resultant $CoFe_2O_4$ and $NiFe_2O_4$, which were 35 and 41 nm, respectively. Fig. 2b indicates the XRD pattern of PPy/CNT/$CoFe_2O_4$.

Because there was no significant change before and after pyrrole polymerization on $NiFe_2O_4$ and $CoFe_2O_4$ in composites, we could confirm that the polymerization reaction had no observable influence on the crystalline structure of these nanoparticles.

The thermal stability of the nanocomposite was considered by TGA. As can be easily perceived from Fig. 3, CNTs are stable in the range of ~50–800 °C. There is obvious weight loss in the two temperature ranges, 220–270 °C and higher than 550 °C. This is because of the decomposition of PPy and CNT respectively. Fig. 3 demonstrates that the ternary nanocomposite is more stable than PPy.

3.1.3. Energy-dispersive spectroscopy analysis

Energy-dispersive spectroscopy (EDS) investigation was also conducted to determine the weight percent of magnetic nanoparticles in the synthesized nanocomposites. According to the EDS measurement (Fig. 4), the content of Fe, Co, and O in $CoFe_2O_4$/PPy and PPy/CNT/$CoFe_2O_4$ is 88.9, 3.4, and 7.8 wt % and 54.3, 18.6, and 27.1 wt %, respectively, which is in accordance with the XRD results. From Fig. 4, it

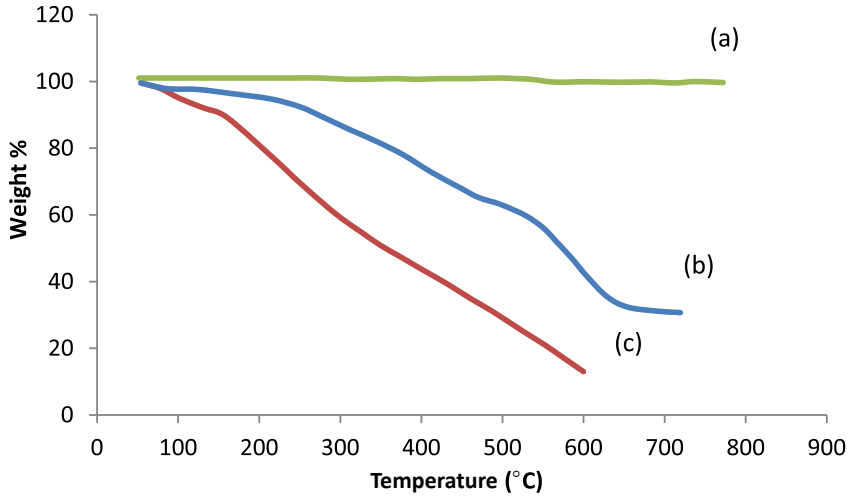

Fig. 3. TGA curves of (a) CNTs, (b) PPy/CNT/$NiFe_2O_4$, and (c) PPy.

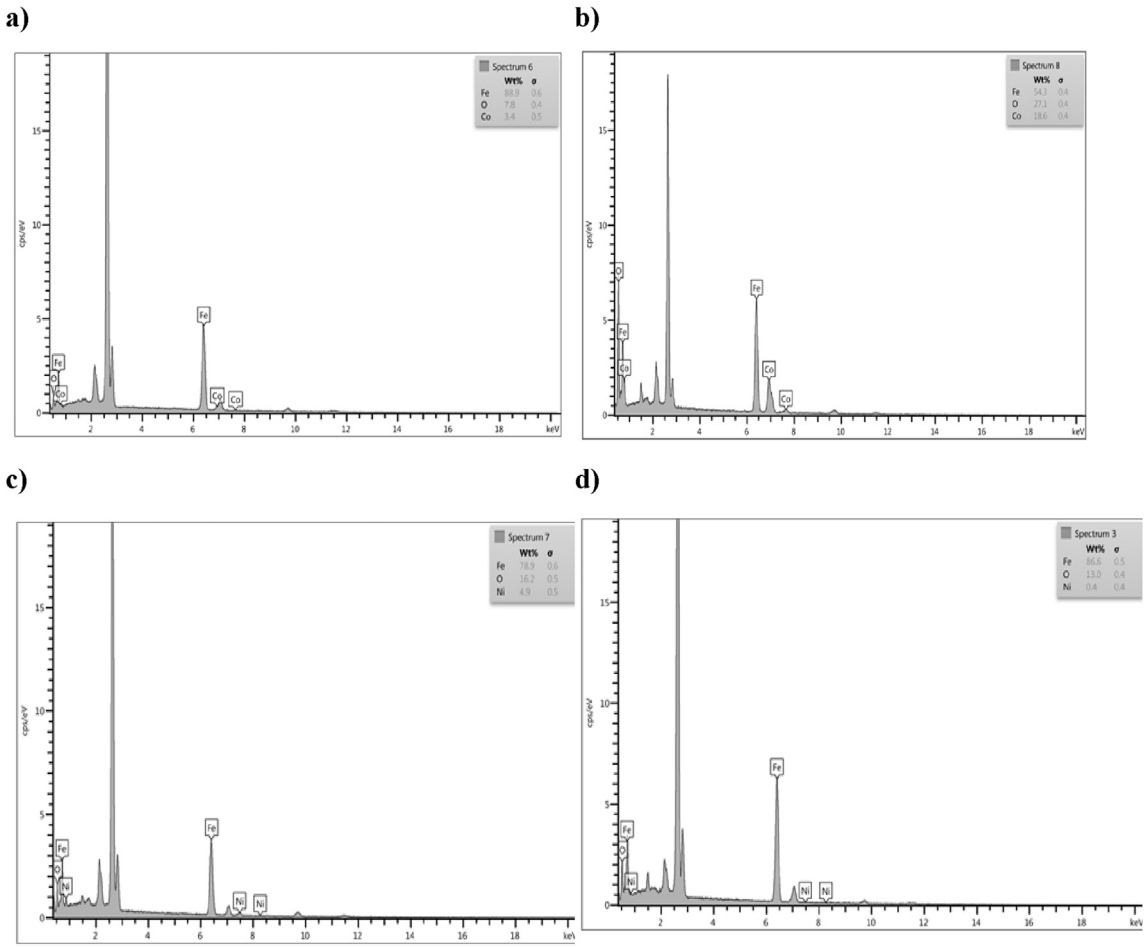

Fig. 4. EDS images of (a) PPy/$CoFe_2O_4$, (b) PPy/CNT/$CoFe_2O_4$, (c) PPy/$NiFe_2O_4$, and (d) PPy/CNT/$NiFe_2O_4$.

can be noticed that similar nanocomposites with Ni content follow the same trend; for instance, the contents of Fe, Ni, and O in $NiFe_2O_4$/PPy and PPy/CNT/$NiFe_2O_4$ are 78.9, 4.9, and 16.2 wt % and 86.6, 13, and 0.4 wt %, respectively, which is in accordance with the XRD results.

In Fig. 4, EDS spectrum confirmed the presence of Fe, Co, and O in PPy/CNT/$CoFe_2O_4$, and Fe, Ni, and O in PPy/CNT/$NiFe_2O_4$. On the basis of these findings, one can induce that the PPy/CNT/$NiFe_2O_4$ and PPy/CNT/$CoFe_2O_4$ composites have been successfully obtained.

ICP-OES is a highly efficient method for determination of metals because of its well-known characteristics. These include satisfactory precision, low detection limit, and relatively small influence of the matrix upon signal in comparison with other used methods, for example, atomic absorption spectroscopy (AAS) [49,50].

In this work, metal concentrations were quantified using ICP-OES at the wavelength of ~220–240 nm. The concentrations of Ni and Fe in $NiFe_2O_4$/PPy and PPy/CNT/$NiFe_2O_4$ are 1124, 18,032 and 286, 59,893 ppm, respectively. The content of Co and Fe in $CoFe_2O_4$/PPy and PPy/CNT/$CoFe_2O_4$ are 953, 21,893 and 9260, 25,342 ppm, respectively.

3.1.4. Morphology study by SEM

Morphology was determined by SEM, undertaken by Philips XL-30 ESEM equipped with an energy-dispersive X-ray (EDX). As expected, a significant difference between the composite and pure PPy was only revealed by high-resolution SEM [51]. As seen in the structural morphology of the synthesized PPy (Fig. 5a), it has a small cubic crystal structure, which can be clearly observed with less magnification. By adding the desired nanoparticles, $CoFe_2O_4$ and $NiFe_2O_4$ come into being with more regularity in a cubic crystal structure toward pure PPy, albeit both pure PPy and prepared composites exhibited cubic morphology. Fig. 5c shows PPy/CNT/$CoFe_2O_4$; along with polymerization, CNT and $CoFe_2O_4$ nanoparticles appeared placed in the PPy matrix. CNT exhibited wire-like morphology between the PPy matrix, which confirms the formation of a nanocomposite. The prepared nanocomposite shows enhanced porosity as compared to pure PPy.

3.1.5. Transmission electron microscopy

Fig. 6 shows TEM of the resultant nanocomposites, which were obtained using a Philips EM208 TEM with an accelerating voltage of 200 kV. According to Fig. 5a,

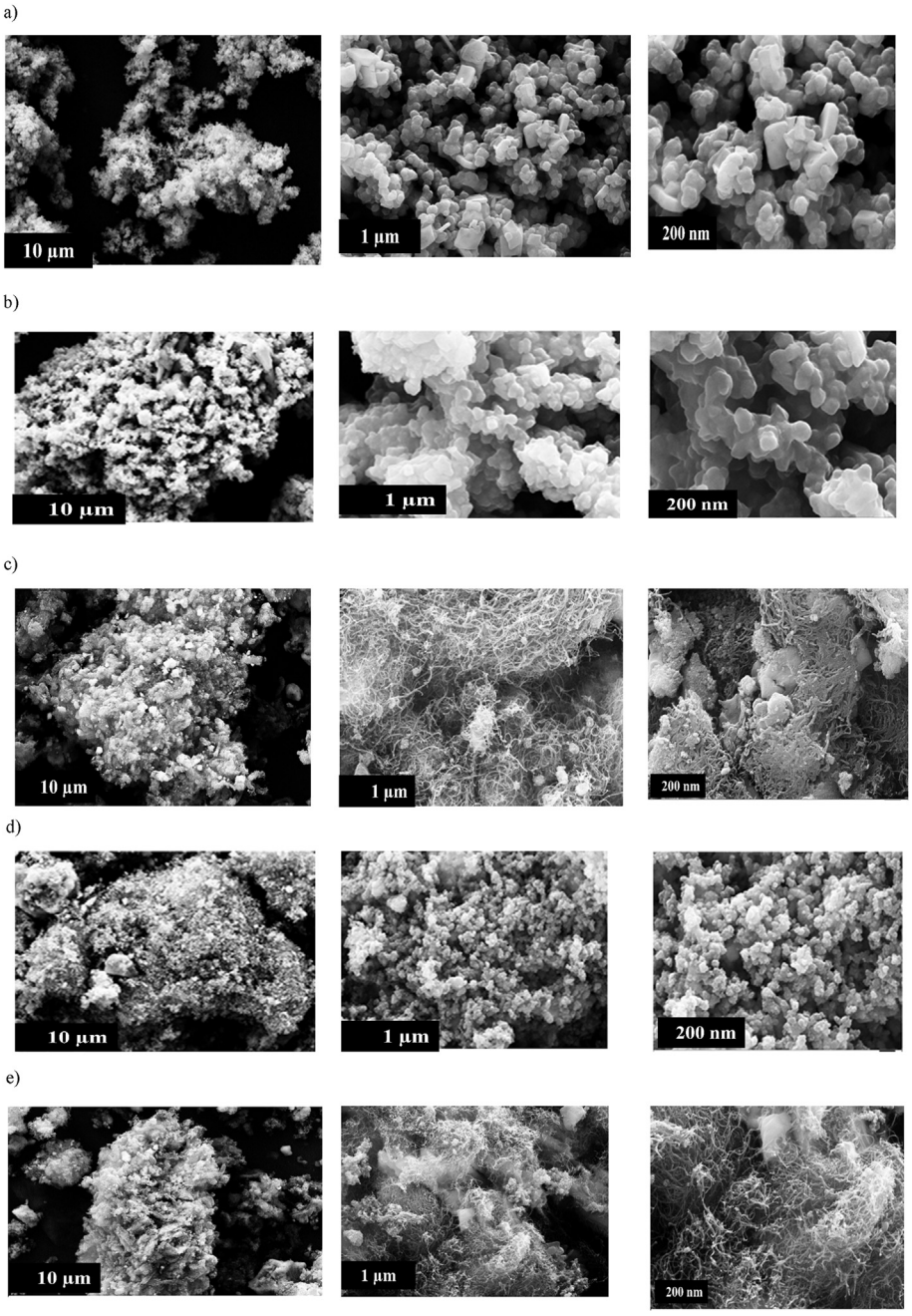

Fig. 5. SEM images (10 µm, 1 µm, and 200 nm) of (a) PPy, (b) PPy/$CoFe_2O_4$, (c) PPy/CNT/$CoFe_2O_4$, (d) PPy/$NiFe_2O_4$, and (e) PPy/CNT/$NiFe_2O_4$.

magnetic nanoparticles are trapped within PPy that are formed in the grid shape. As can be clearly found from Fig. 6b, wire-like CNT appears placed between mesh-like PPy. Fig. 6 shows a colony of magnetic nanoparticles, which are captured inside the polymer network.

3.2. Magnetic properties

3.2.1. Vibrating sample magnetometer analysis

Vibrating sample magnetometer systems were used to measure the magnetic properties of materials as a function of magnetic field, temperature, and time. They are ideally suited for research and development, production testing, and quality and process control. Powders, solids, liquids, single crystals, and thin films are all readily accommodated in a vibrating sample magnetometer [52].

The magnetic properties of PPy/CNT/$NiFe_2O_4$ and PPy/CNT/$CoFe_2O_4$ are shown in Fig. 7a and b, respectively. As can be seen from Fig. 7, the nanocomposite containing $NiFe_2O_4$ and $CoFe_2O_4$ shows ferromagnetic behavior. The saturation magnetization values of the composite containing $NiFe_2O_4$ and $CoFe_2O_4$ are 4.3 and 4.05 emu/g,

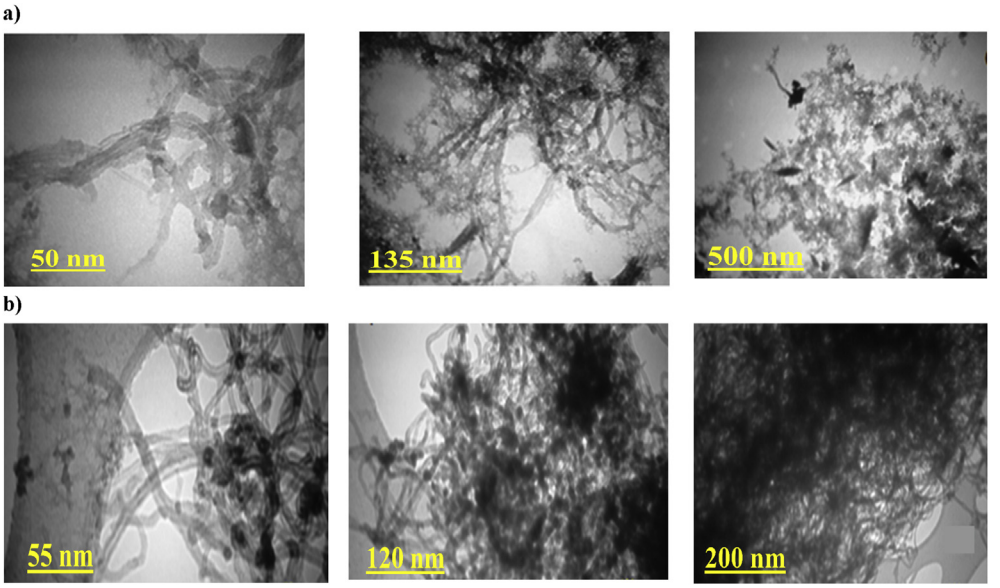

Fig. 6. TEM images of (a) PPy/CNT/$NiFe_2O_4$ and (b) PPy/CNT/$CoFe_2O_4$.

respectively, and their coercivity values are 7.4 and 215.5 Oe, respectively. As shown, the polymer nanocomposite containing $CoFe_2O_4$ has a higher coercivity than the other one. A probable reason could be that the magnetic moments of $CoFe_2O_4$ nanostructures are more decayed in the PPy matrix than that of the $NiFe_2O_4$. Therefore, a higher magnetic field is essential to align the single domain nanoparticles in the field direction. As seen in Fig. 7, in the case of magnetic saturation the trend is quite apposite. The nanocomposite containing $NiFe_2O_4$ has a higher magnetic saturation, and, as a result, it is expected that the microwave absorption of this nanocomposite will be high.

3.3. Microwave reflection loss

To indicate microwave absorption properties of the synthesized samples, the reflecting loss values of an absorbent were calculated through the transmission line theory. To this objective, the reflection loss value and transmission parameters, and absorption and reflection of EM waves from the surface of samples were measured and calculated using an HP 8510B Network Analyzer (Helwlett −Packard) calibrated in the transmission mode to obtain reflection and transmission coefficients. Because each sample was larger than the waveguide opening, the problem of losses at corners and edges was eliminated. Consequently, accurate and reproducible reflection and transmission measurements were achieved [1].

Microwave reflectivity of prepared nanocomposites was investigated in the frequency range 2−18 GHz [1]. The reflection loss of PPy/CNT/$NiFe_2O_4$ (the weight of composite particles in the epoxy resin was 5 wt %) of a layer thickness of 2 mm is presented in Fig. 8a. As seen in Fig. 7a, this sample has a maximum reflection loss of −33 dB at 6.4 GHz. Moreover, it has some other flagship absorptions of −6.2 dB at 29 GHz and −4.4 dB at 28 GHz.

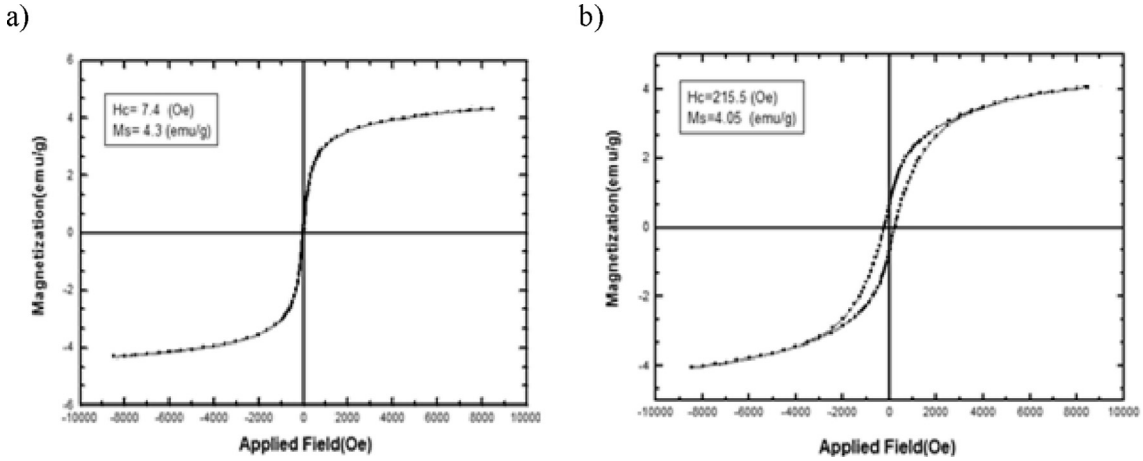

Fig. 7. Magnetization curves of (a) PPy/CNT/$CoFe_2O_4$ and (b) PPy/CNT/$NiFe_2O_4$.

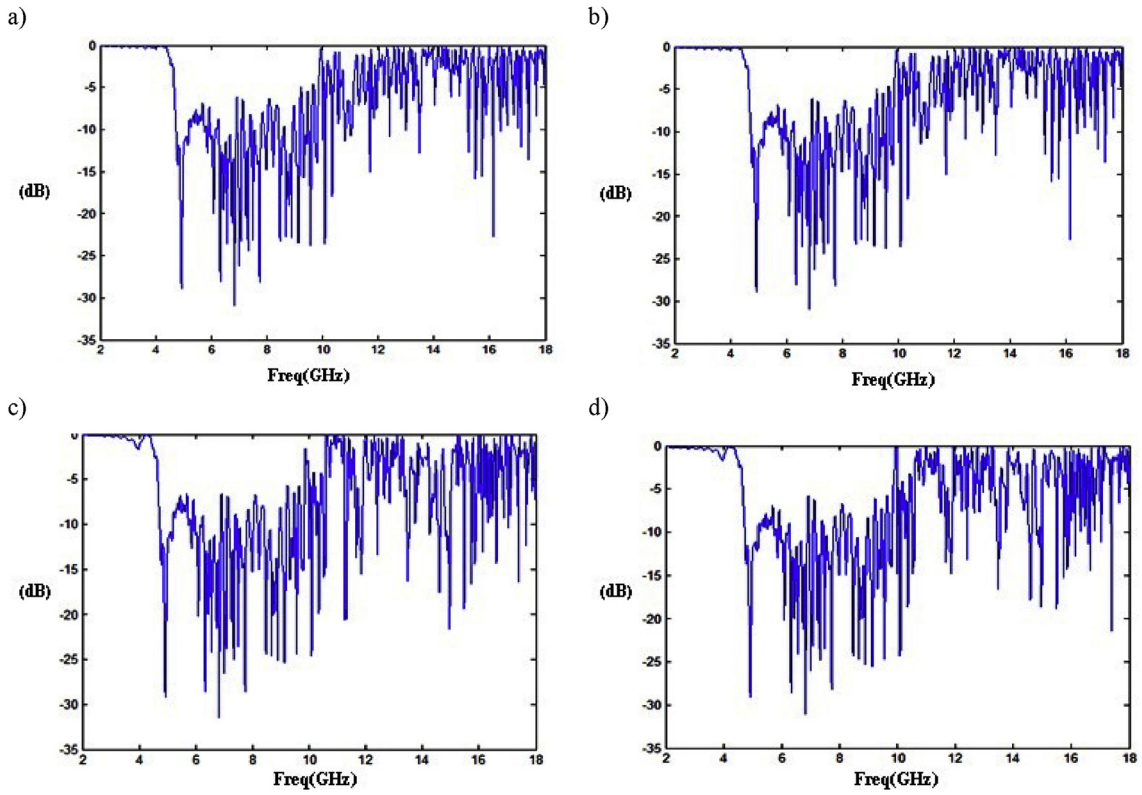

Fig. 8. Microwave reflection losses of (a) PPy/CNT/$NiFe_2O_4$ (2 mm, 5 wt %), (b) PPy/CNT/$NiFe_2O_4$ (0.5 mm, 20 wt %), (c) PPy/CNT/$NiFe_2O_4$ (2 mm, 20 wt %), and (d) PPy/CNT/$CoFe_2O_4$ (1.25 mm, 12.5 wt %).

In this sample, with a decrease in layer thickness to 0.5 mm and an increase in the weight of composite particles in epoxy resin to 20 wt %, almost similar results were achieved (Fig. 8b).

The reflection loss of PPy/CNT/$CoFe_2O_4$ (the weight of composite particles in epoxy resin was 12.5 wt %) at a layer thickness of 1.25 mm is presented in Fig. 8d. As seen in Fig. 8d, this sample has maximum reflection loses of −33 dB at 6.4 GHz. It also has two other indicator absorptions of −6.2 dB at 27 GHz and −4.5 dB at 29 GHz.

As shown in Fig. 8, in all cases the microwave absorption of the polymer matrix was increased by adding the nanomagnet to the polymer matrix. The other factor that affects the microwave absorption of synthesized polymer nanocomposite is morphology. One can plainly see that a higher surface-to-volume ratio of magnetic nanostructures also increases microwave absorption. Therefore, because of their wire-like morphology, $NiFe_2O_4$ and $CoFe_2O_4$ make a higher surface-to-volume ratio and consequently help to increase the microwave absorption amount. Furthermore, because the wire-like structures have a small dimension, they spread easily in the polymer matrix; consequently, the amount of microwave absorption of the polymer increases significantly. As we can see from Fig. 8, microwave absorption of PPy/CNT/$NiFe_2O_4$ is higher toward the PPy/CNT/$CoFe_2O_4$ nanocomposite. This can be because of the higher magnetic saturation of the PPy/CNT/$NiFe_2O_4$ nanocomposite. In fact, magnetic materials with high saturation improve the microwave absorption.

4. Conclusion

In the present work two different composites, PPy/CNT/$CoFe_2O_4$ and PPy/CNT/$NiFe_2O_4$, were successfully synthesized by the in situ polymerization method. This is novel, cost effective, and easily scaled. The evaluation results of different analysis, FT-IR, elemental analysis, TEM, SEM, EDS, and XRD, showed that the desired nanocomposites were successfully prepared. As mentioned above, the saturation magnetization (M_s) and coercivity values of the $CoFe_2O_4$ and $NiFe_2O_4$ nanoparticles display a reduction trend toward those of the prepared $CoFe_2O_4$/PPy/CNT and $NiFe_2O_4$/PPy/CNT nanocomposites. This could be because of the polymerization of the monomer and pyrrole on the surface of nanoparticles. According to the XRD results, both the synthesized nanocomposites have the spinel structure. On the basis of the investigation of microwave reflection loss of prepared nanocomposites, it was found that its value increased with the increase in the PPy content and polymerization on the surface.

The results also show that microwave absorption improves significantly as magnetic nanomaterials and CNT in the polymer matrix increase. Moreover, it was found that the morphology of the magnetic nanomaterials plays a critical role in microwave absorption property. Also, in this work, two magnetic nanomaterials were applied for enhancement of microwave absorption, adding CNT in the polymer matrix leads to the improvement in microwave absorption.

Acknowledgments

Support from the Amirkabir University is gratefully acknowledged.

References

[1] K. Akif, W. Joeuns, C. Ray, S.M. Anand, E.B. Geoffrey, J. Appl. Polym. Sci. 54 (1994) 269–278.
[2] J. Unsworth, A. Kaynak, B.A. Lunn, G.E. Beard, J. Mater. Sci. 28 (1993) 3307–3312.
[3] M. Yu, C. Liang, M. Liu, X. Liu, K. Yuan, H. Cao, R. Che, J. Mater. Chem. C 2 (2014) 7275–7283.
[4] C. Liang, C. Liu, H. Wang, L. Wu, Z. Jiang, Y. Xu, B. Shen, Z. Wang, J. Mater. Chem. A 2 (2014) 16397–16402.
[5] Z. Yang, Z. Li, L. Yu, Y. Yang, Z. Xu, J. Mater. Chem. C 2 (2014) 7583–7588.
[6] A. Kumar, A.P. Singh, S. Kumari, P.K. Dutta, S.K. Dhawan, A. Dhar, J. Mater. Chem. A 2 (2014) 16632–16639.
[7] A.P. Singh, M. Mishra, P. Sambyal, B.K. Gupta, B.P. Singh, A. Chandra, S.K. Dhawan, J. Mater. Chem. A 2 (2014) 3581–3593.
[8] Y. Ruey-Bin, R. Madhusudhana, C. Chi-Jung, C. Po-An, C. Jem-Kun, C. Chung-Chieh, Chem. Eng. J. 285 (2016) 497–507.
[9] A. Houdayer, R. Schneider, D. Billaud, J. Ghanbaja, J. Lambert, Synth. Met. 151 (2015) 165–174.
[10] A. Sarkar, S. Kapoor, G. Yashwant, H.G. Salunke, T. Mukherje, J. Phys. Chem. B 109 (2005) 7203–7207.
[11] Q.L. Yang, J. Zhai, L. Feng, Y.L. Song, M.X. Wan, L. Jiang, W.G. Xu, Q.S. Li, Synth. Met. 135–136 (2003) 819–820.
[12] K. Suri, S. Annapoorni, R.P. Tandon, C. Rath, V.K. Aggrawal, Curr. Appl. Phys. 3 (2003) 209–213.
[13] A. Chen, H. Wang, B. Zhao, X. Li, Synth. Met. 139 (2003) 411–415.
[14] W. Chen, X. Li, G. Xue, Z. Wang, W. Zou, Appl. Surf. Sci. 218 (2003) 216–222.
[15] A.A. Novakova, V.Y. Lanchinskaya, A.V. Volkov, T.S. Gendler, T.Y. Kiseleva, M.A. Moskvina, S.B. Zezin, J. Magn. Magn. Mater. 258–259 (2003) 354–357.
[16] R.N. Singh, B. Lal, M. Malviya, Electrochim. Acta 49 (2004) 4605–4612.
[17] Z. Hu, H.X. Zhao, C. Kong, Y.Y. Yang, X.L. Shang, L.J. Ren, Y.P. Wang, J. Mater, Sci. Mater. Electron. 17 (2006) 859–863.
[18] M.H. Sousa, F. Atourinho, J. Depeyrot, G.J. da-Silva, M.C. Lara, J. Phys. Chem. B 105 (2001) 1168–1175.
[19] K. Raj, R. Moskowitz, R. Casciari, J. Magn. Magn. Mater. 149 (1995) 174–180.
[20] T. Hyeon, Y. Chung, J. Park, S.S. Lee, Y.W. Kim, B.H. Park, J. Phys. Chem. B 106 (2002) 6831–6833.
[21] R.V. Mehtha, R.V. Upadhyay, B.A. Dasanacharya, P.S. Goyal, K.S. Rao, J. Magn. Magn Mater. 132 (1994) 153–158.
[22] M.H. Kryder, Mater. Res. Soc. Bull. 21 (1996) 17–22.
[23] D.G. Mitchell, J. Magn. Reson. Imag. 7 (1997) 1–4.
[24] C. Xuebo, G. Li, Nanotechnology 16 (2005) 180–185.
[25] X. Huang, Z. Chen, Mater. Res. Bull. 40 (2005) 105–113.
[26] R.H. Kodama, J. Magn. Magn. Mater. 200 (1999) 359–372.
[27] J.G. Lee, J.Y. Park, Y.J. Oh, C.S. Kim, J. Appl. Phys. 84 (1998) 2801–2804.
[28] A.K. Giri, K. Pellerin, W. Pongsaksawad, M. Sorescu, S. Majetich, IEEE Trans. Magn. 36 (2000) 3029–3031.
[29] A. Pui, D. Gherca, G. Carja, J. Nanomater. Bios. 6 (2011) 1783–1791.
[30] J. Deng, C. He, Y. Peng, J. Wang, X. Long, P. Li, A.S. Chan, Synth. Met. 139 (2003) 295–301.
[31] J.C. Aphesteguy, S.E. Jacobo, Phys. B 354 (2004) 224–227.
[32] J. Deng, X. Ding, W. Zhang, Y. Peng, J. Wang, X. Long, P. Li, A.S. Chan, Polymer 43 (2002) 2179–2184.
[33] L. Jing, W. Meixiang, Polym. Chem. 38 (2000) 2734–2739.
[34] J. Gass, P. Poddar, J. Almand, S. Srinath, H. Srikanth, Adv. Funct. Mater. 16 (2006) 71–75.
[35] G. Kousik, S. Pitchumani, N.G. Renganathan, Prog. Org. Coat. 43 (2001) 286–291.
[36] D.V. Brezoi, R.M. Ion, Sens. Actuators, B 109 (2005) 171–175.
[37] L. Bao, J.S. Jiang, Phys. B 367 (2005) 182–187.
[38] M.S. Cao, J. Yang, W.L. Song, D.Q. Zhang, B. Wen, H.B. Jin, Z.L. Hou, J. Yuan, ACS Appl. Mater. Interfaces 4 (2012) 6949–6956.
[39] P. Liu, Y. Huang, L. Wang, W. Zhang, J. Alloys Compd. 573 (2013) 151–156.
[40] J. Luo, D. Gao, J. Magn. Magn. Mater. 368 (2014) 82–86.
[41] J. Luo, Y. Xu, W. Yao, C. Jiang, J. Xu, Compos. Sci. Technol. 117 (2015) 315–321.
[42] Y. Xu, J. Luo, W. Yao, J. Xu, T. Li, J. Alloys Comp. 636 (2015) 310–316.
[43] J. Luo, P. Shen, W. Yao, C. Jiang, J. Xu, Nanoscale Res. Lett. 11 (2016) 141.
[44] Y. Du, W. Liu, R. Qiang, Y. Wang, X. Han, J. Ma, P. Xu, ACS Appl. Mater. Interfaces 6 (2014) 12997–13006.
[45] S. Machida, S. Miyata, Synth. Met. 31 (1989) 311–318.
[46] Y. Li, D. Chen, X. Liu, Y. Zhou, Q. Zhuang, R. Cai, K. Zhang, Compos. Sci. Technol. 100 (2014) 212–219.
[47] H.B. Gu, Y.D. Huang, X. Zhang, Polymer 53 (2012) 801–809.
[48] G.A. Dorofeev, A.N. Streletskii, I.V. Povstugar, A.V. Protasov, E.P. Elsukov, Colloid J. 74 (2012) 710–720.
[49] R. Cornelirs, Sci. Total Environ. 71 (1988) 269–283.
[50] D. Beauchemidn, J.W. Mclaren, S.S. Bermanj, J. Anal. At. Spectrom. 3 (1988) 775–780.
[51] Z.C. George, S.P. Milo, C. Dan, D. Gemma, Z. Wuzong, J.F. Derek, H.W. Alan, Adv. Mater. 12 (2000) 522–525.
[52] S. Foner, Rev. Sci. Instrum. 30 (1959) 548–557.